Alessandro Corsini

Franco Rispoli

Dipartimento di Meccanica e Aeronautica,
Università di Roma "La Sapienza,"
Via Eudossiana 18,
I-00184 Rome, Italy

A. G. Sheard
Fläkt Woods Limited,
Tufnell Way,
Colchester CO4 5AR, UK

Shaping of Tip End-Plate to Control Leakage Vortex Swirl in Axial Flow Fans

This paper reports on quantitative tests of passive techniques for rotor-tip noise control in low-speed axial flow fans, based on blade-tip modifications involving the addition of antivortex appendages as end-plates. The end-plate thickness chordwise distribution is determined to control the chordwise evolution of the leakage vortex rotation number. The results confirm that the new end-plate configurations provide a mechanism by which leakage vortex bursting can be avoided. As such, the modified rotors represent an effective means of passive control of vortex breakdown. [DOI: 10.1115/1.3145017]

1 Introduction

Blade-tip aerodynamics are largely determined by (i) nonlinear interactions of tip-leakage flows, (ii) skewed end-wall boundary layers, and (iii) secondary blade passage flows. The complexity of these blade-tip aerodynamic mechanisms determines the rotor operating margin in tip-stalling rotors because the aerodynamics establish the blade spanwise loading and loss distributions and the turbomachine's aero-acoustic signature [1–3]. As demonstrated by Ganz et al. [4], the physical mechanisms governing the tip-region flow around blades in turbomachinery compressors also apply in industrial ventilation and cooling fans. The diminished performance associated with the presence of these flow mechanisms has prompted the designers of fans and compressors to devise new design features that minimize the adverse aerodynamic effects of tip gap. In doing so, their objective is to manage the tip-clearance flow in a manner that reduces the self-generated noise without sacrificing aerodynamic efficiency. This objective can be achieved either by reducing the leakage flow rate or by enhancing the primary-secondary flow momentum transfer.

For industrial fans and turbomachinery compressors, research efforts in pursuit of the above objective can be categorized into two approaches. The use of casing treatments in the shroud portion over the blade tip was first reported in the early 1970s. This provided an improved stable flow range by weakening the tip-leakage vortex (TLV). Noticeable contributions have reported the use of grooves and slots [5,6] and stepped tip gaps [7]. More specifically, in terms of fan technology, recirculating vanes and annular rings were proposed as antistall devices [8]; indeed, these are now in routine commercial operations.

A second broad approach consists of passive control techniques. Various passive approaches were proposed with concepts based on blade-tip modifications by means of antivortex appendages, such as those investigated by Quinlan and Bent [9], or those advocated by patents for industrial patents for ventilating fans [8,10–12].

Recently, Corsini et al. [13–15] investigated the application of profiled end-plates to the blade tips of a family of commercially available industrial fans. They reported benefits in terms of aerodynamic and aero-acoustic performance as a result of the adoption of these modified blade-tip configurations. In particular, the adoption of a constant-thickness end-plate that had originally been designed at Fläkt Woods Ltd. (Colchester, UK) for an industrial fan (designated as AC90/6/TF) provided an effective control of leakage-flow phenomena over the fan operating range. However, in spite of the aero-acoustic gains, the aerodynamic tests of the AC90/6/TF configuration revealed a diminution in performance in association with the occurrence of leakage vortex bursting over the tip end-plate. This breakdown was characterized by the abrupt expansion of the swirling core into a bubblelike circulatory zone.

The aim of the present paper is to present a new configuration of the thickness distribution of the antivortex tip end-plate and to provide details of its design concept [16]. This new configuration consists of a variation in thickness, which aims to control the chordwise evolution of the leakage vortex rotation number. The new end-plate configuration thus provides a passive control mechanism whereby leakage vortex bursting can be avoided. Vortex breakdown is an intriguing phenomenon of practical importance. It occurs in swirling flows and, depending on the application, can be considered as a positive or negative phenomenon. Control of the phenomenon was of interest to scholars for 2 decades and continues to be an active area of research—especially in aeronautical applications (for example, delaying delta wing vortices or accelerating trailing tip vortices [17]) and in combustors, valves, and cyclones [18]. In the present study, the modified configuration aims to influence the onset of vortex breakdown by the use of a variable chordwise end-plate thickness distribution. The aim is to promote an enhancement of near-axis swirl [19,20] by influencing the momentum transfer from the leakage flow and by inducing some waviness into the leakage vortex trajectory, as suggested by Srigrarom and Kurosaka [21] with respect to the delta-wing platform design.

The remainder of this paper is organized as follows. First, the family of test fans is described and the background quantitative experimental investigations are summarized. This is followed by a survey of leakage flow in the tip region of fan AC90/6/TF to provide evidence of the presence of vortex breakdown. The rationale for the proposed end-plate thickness distribution configuration is then briefly described. Section 6 of this paper presents a comparative assessment of the end-plate aerodynamics.

2 Methodology

2.1 Test Fans. The present study was undertaken using a family of commercially available industrial cooling fans. In-service experience had indicated that this family of fans provides good acoustic performance. The fan featured a six-blade unswept rotor, with the blade profiles being a modified ARA-D configuration that was originally designed for propeller applications. The details of the blade profile for the AC90/6 fan are given in Table 1.

The design specifications for both the data and modified rotors studied here are given in Table 2. The blade configurations stud-

Contributed by the International Gas Turbine Institute of ASME for publication in the JOURNAL OF TURBOMACHINERY. Manuscript received August 6, 2008; final manuscript received February 25, 2009; published online March 24, 2010. Review conducted by David Wisler. Paper presented at the ASME Turbo Expo 2008: Land, Sea and Air (GT2008), Berlin, Germany, June 9–13, 2008.

 Copyright © 2010 by ASME

Downloaded 28 May 2010 to 128.113.26.88. Redistribution subject to ASME license or copyright; see http://www.asme.org/terms/Terms_Use.cfm

Table 1 Blade profile of AC90/6 fan

	AC90/6 blade		
	Hub	Midspan	Tip
ℓ/t	1.32	0.52	0.31
Stagger angle (deg)	54	58.8	62
Camber angle (deg)	46	44	41

ied, for data and modified rotors, feature a high tip stagger angle, as is customary for the class of investigated industrial fan operations. This rotor angular setting was chosen to exploit operating point at which the vortex flow near the rotor tip has its most significant effects on the aerodynamic performance and noise characteristics of the investigated fans.

The two configurations studied were (i) the data rotor (AC90/6) and (ii) a modified rotor (designated as AC90/6/TF), which was designed with a view to low noise emission, see Fig. 1. The modified AC90/6/TF rotor blades differed from the data blades in the blade tip vicinity. The configuration of the AC90/6/TF blade tip, which was originally inspired by designs developed for tip-vortex control and drag reduction in aircraft wings and catamaran hulls, differed from the data fan by the addition of an end-plate. This end-plate ran along the blade pressure surface and ended on the blade trailing edge (te) with a square tail. The addition of this end-plate means that the blade section was locally thickened by a factor of 3 with respect to the maximum thickness at the tip of the data blade. This dimension was determined in proportion to the radial dimension of the leakage vortex chosen on the basis of previous studies, both of axial compressors [22] and fans [23], in which the vortex dimension to be controlled was estimated to be 0.1–0.2 blade spans.

2.2 Background Investigations. Recent studies by Corsini et al. [13–15] have assessed the performance associated with the modified end-plate configuration of the AC90/6/TF rotor. These studies have demonstrated that the modified end-plate configuration effectively controlled the leakage-flow phenomena over the fan operating range. In doing so, the end-plate improved the three-dimensional (3D) loss behavior, moved the peak efficiency plateau toward the lower flow rate, and markedly reduced the fan's aero-acoustic signature.

Table 3 shows the overall aerodynamic and acoustic performance for two operating points: (i) the near-design condition (designated as "*D* point") with a volume flow rate of 7 m^3/s and (ii) a near-peak pressure condition (designated as "*P* point") with a volume flow rate of 6 m^3/s. In addition, the overall noise performance is provided in terms of the unweighted and *A*-weighted sound-power levels (SWLs) at a distance of 6 m from the fan outlet, Table 3.

Table 2 Design specifications of AC90/6 family of fans

Design specifications	
Blade number	6
Blade tip stagger angle (deg)	62
Hub-to-casing diameter ratio ν	0.22
Hub diameter D_h (mm)	200.0
Casing diameter D_c (mm)	907
Rotor tip clearance χ (% span)	1.0
Rotational frequency (rpm)	900–935

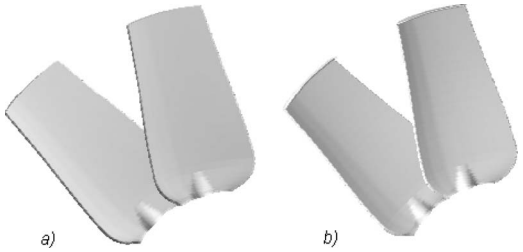

Fig. 1 Fan rotors: (*a*) data fan and (*b*) modified AC90/6/TF fan

Table 3 Overall aerodynamic and acoustic performance of fans

	Data rotor		AC/90/6/TF rotor	
Aerodynamic	Δp_{stat} (Pa)	η	Δp_{stat} (Pa)	η
D point	134.8	0.49	126.2	0.51
P point	184.4	0.44	179.4	0.49
Acoustic	Unweighted SWL (dB)	*A*-weighted SWL (dB(A))	Unweighted SWL (dB)	*A*-weighted SWL (dB(A))
D point	72.38	70.85	70.17	66.92
P point	72.72	71.85	69.66	67.44

2.3 Numerical Method. The Reynolds-averaged Navier–Stokes equations were solved by an original parallel multigrid (MG) finite element flow solver [24]. The fluid dynamics of incompressible 3D turbulent flows in a rotating frame of reference was modeled with a topology-free low-Reynolds variant of a nonlinear k-ε model [25].

The numerical integration of partial differential equations (PDEs) was based on a stabilized Petrov–Galerkin formulation to control the instability that affects the advective-diffusive incompressible flow limits and the momentum and turbulent scale-determining equations. The latter related, respectively, to the Coriolis acceleration and to the dissipation/destruction terms in the turbulent scale-determining equations [25]. Equal-order linear interpolation spaces (Q1-Q1) were used for primary-turbulent and constrained variables, which effectively eliminated the undesirable pressure-checkerboarding effects. A hybrid full-linear MG accelerator was built into the in-house overlapping parallel solver. This numerical technique was previously validated with transitional compressor cascade flows and with high-pressure industrial fan rotors [14,23,24].

The Krylov iterations in the smoothing/solving of the MG phases were parallelized using an original additive domain-decomposition algorithm. The message-passing operations were managed using message-passing interface (MPI) libraries. Using this technique, the fully coupled solution of the subdomain problem involves an efficient nonconventional use of Krylov subspace methods. The preconditioned Generalized Minimal Residual (GMRES)(5) and GMRES(50) algorithms were used, respectively, as smoother and core solver.

2.4 Fan Rotor Modeling and Boundary Conditions. The mesh was built in a nonorthogonal body-fitted coordinate system by merging two structured h-type grid systems: (i) mesh in the main flow region (surrounding the blade) and (ii) embedded mesh in the tip-gap region.

The mesh had $154 \times 68 \times 58$ nodes in the axial, pitch, and spanwise directions, respectively. In the axial direction, the node distribution consisted of 20% of nodes upstream of the leading edge (le), 50% of nodes in the blade passage, and 30% of nodes downstream of the blade passage. Additionally, there were 14 grid nodes to model the tip clearance along the span. The computational grid had an adequate clustering toward the solid boundaries, with the ratio of minimum grid spacing on solid walls to midspan

Downloaded 28 May 2010 to 128.113.26.88. Redistribution subject to ASME license or copyright; see http://www.asme.org/terms/Terms_Use.cfm

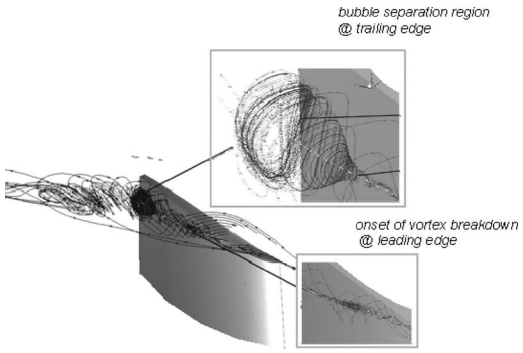

Fig. 2 Streamlines in the rotor tip gap at *D* operating point and vortex bursting visualization

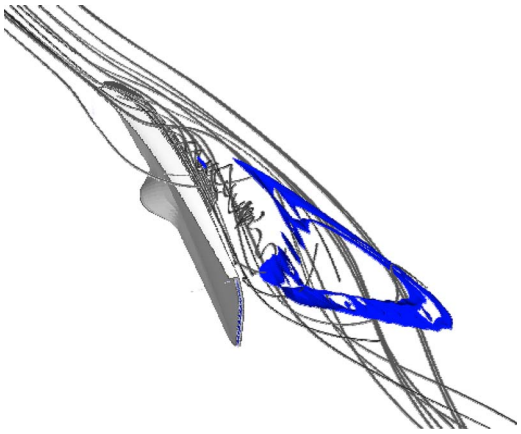

Fig. 3 Streamlines and vortex axial velocity isosurface ($w_{a\mathrm{TLV}}=0$) in the rotor tip gap at *D* operation

blade chord being set at 2×10^{-3} on the blade tip, casing wall, and blade surfaces. The grid refinement toward the solid surfaces controlled the dimensionless distance δ^+ value at about 1 on the first node row.

2.5 Boundary Conditions and Investigated Flow Conditions. Standard boundary conditions were adopted in accordance with those used in recent quantitative studies of high-performance fans [23].

The Dirichlet conditions for the relative velocity components were imposed at the inflow section, half a midspan chord upstream of the leading edge. The velocity profile was obtained from the flow simulation in an annular passage of identical hub-to-casing diameter ratio that included an upstream spinner cone. The inlet distribution of the turbulent kinetic energy (k) was obtained from an axisymmetric turbulence intensity (TI) profile derived from previous studies of ducted industrial fans. The TI profile featured a nearly uniform value in the core region (about 6%), which increased markedly approaching the endwalls (about 10%). The inlet profile of turbulence energy dissipation was based on the length scale (l_ε) set to 0.01 of the rotor pitch at midspan. Flow periodicity upstream and downstream of the blading, and Neumann outflow conditions (homogeneous for k and ε and nonhomogeneous for the static pressure), completed the set of boundary data.

The fan leakage-flow patterns for the tested fans were then investigated and compared under near-design conditions (D) with a volume flow rate of 7 m^3/s and a global flow coefficient Φ of 0.278. The Reynolds number (based on tip diameter and rotor tip speed) was 8.3×10^5 for normal air conditions.

3 Leakage Vortex Breakdown

3.1 Evidence of Vortex Breakdown. As previously noted, Corsini et al. [13–15] assessed the performance gains that are offered by the modified end-plate concept of rotor AC90/6/TF. In particular, the leakage flow was studied to identify the mechanisms that produce the improved aero-acoustic signature. According to Corsini et al. [26], the aerodynamic appendages at the blade tip gave rise, under near-design operating conditions, to a bursting of the tip-leakage vortex. To provide greater insight into this phenomenon, the 3D streamline behavior in the tip gap of rotor AC90/6/TF was visualized (see Fig. 2) under D operating conditions.

The antivortex effect produced by the end-plate acted as a physical obstacle to the pressure surface-flow migration and preserved the pressure-side tip vortex, thus producing a vena contracta effect. As a consequence, the leakage flow (as visualized with 3D streamlines) revealed that the reduction in flow leaking altered the swirl-to-axial vortex velocity component ratio, which gave rise to an unseparated bubble-core about midchord followed by a large bubble-type separation in the aft portion of the blade passage. This finding was in accordance with the existence of a vortex breakdown (because the flow reversal is indicative of the critical bursting phenomenon [27]). Moreover, according to Leibovich [28], the appearance of the vortex bursting in the bubble form can be interpreted as a consequence of a sufficiently large swirl level.

As observed by Escudier and Zehnder [29] and Inoue and Furukawa [30], the bubble form of the vortex breakdown is increasingly steady with the level of swirl, which supports the proposition that the bubble-separation core (provided by the steady simulation) is evidence of the occurrence of tip-leakage vortex breakdown. The midchord bubble core can therefore be considered as evidence of the onset of the bursting of the rear vortex.

To assess the veracity of the above conjecture, tip-leakage vortex axial velocity zero isosurfaces were drawn, as shown in Fig. 3, together with the 3D streamlines in the blade-tip region. A zero $w_{a\mathrm{TLV}}$ core was located by coincidence with the unseparated bubble-core (see Fig. 2), which was identified as the onset of the vortex breakdown. This finding is in accordance with the observation of Spall et al. [17], who first identified the presence of a stagnation point along the vortex axis as a necessary condition for the breakdown to appear. A second (and larger) zero-velocity isosurface, Fig. 2, limits the bursting core featuring the flow reversal.

As a last criterion for the detection of vortex breakdown, the tip-leakage vortex structures were investigated using a normalized helicity (H_n) based on the absolute vorticity [2,30] as a detection tool. H_n was defined and normalized as $H_n=(\xi_i\cdot w_i)/(|\xi||w|)$ with $i=1,\ldots,3$, where ξ_i and w_i are the Cartesian components of the absolute vorticity and relative velocity vectors, and $|\xi|$ and $|w|$ are their norms. When plotting the normalized helicity H_n contours on cross sections, Fig. 4, for the data rotor and the AC90/6/TF rotor, the probing planes were located at 0.25 blade chords, 0.43 blade chords, 0.65 blade chords, 0.89 blade chords, and 1.2 blade chords from the tip-section leading edge. The normalized helicity distribution was then plotted with the vortex cores.

As shown in Fig. 4, the AC90/6/TF rotor (Fig. 4(a)) demonstrated a modified tip-leakage phenomenon in comparison with the data rotor (Fig. 4(b)). In particular, at about midchord, the main tip-leakage vortex featured a gradual reduction in H_n as a result of the weakening of the flow vortex and the deflection of the vortex core. This finding is in accordance with the hypothesis of mass leaking reduction along the chord, which gives rise to leakage-flow structures adjacent to the blade's suction surface. In the aft portion of the blade, the reduction in the flow leaking was such that the main TLV collapsed and became a counterclockwise vortex under the influence of trailing-edge leakage flow streams, which rapidly washed out the vortex behind the rotor. Correspondingly, on the 1.2ℓ plane, no coherent vortex structure was apparent.

Downloaded 28 May 2010 to 128.113.26.88. Redistribution subject to ASME license or copyright; see http://www.asme.org/terms/Terms_Use.cfm

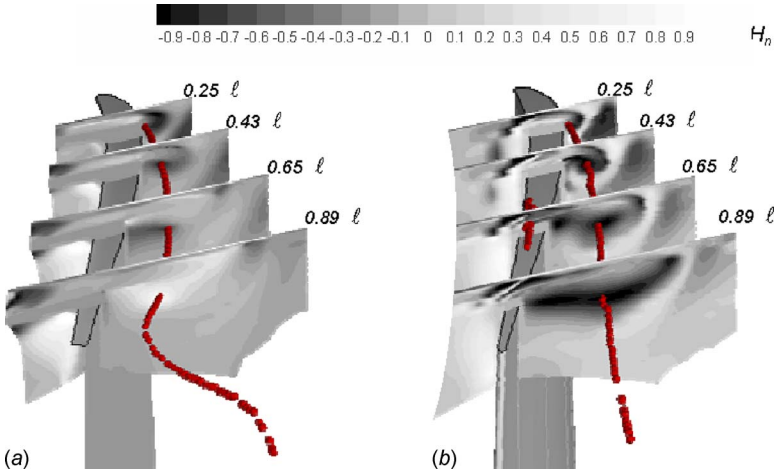

Fig. 4 Normalized helicity H_n contours on cross sections and vortex cores at the tip, *D* operating point: (*a*) AC90/6/TF rotor and (*b*) AC90/6 data rotor

These findings can be considered additional evidence in support of the proposition that vortex breakdown occurred. The most distinctive feature was the helicity inversion, which occurred as a result of the counter-rotation of the vortex exiting from the bursting region. This phenomenon, which is accepted as evidence of vortex breakdown in compressor rotors [30], is consistent with the criterion based on the angle of the velocity and vortex vectors. Several studies have attempted to explain the vortex breakdown on the basis of the behavior of the azimuthal vortex component; in particular, Leibovich [31] stated that a change in sign of the azimuthal vortex is definitive evidence of the existence of vortex breakdown.

3.2 Vortex Breakdown Rossby Number Analysis. Almost all of the studies on vortex breakdown, including those on linear stability and phase velocity [32] and those on wave trapping [33], have attempted to identify a critical condition for the appearance of vortex bursting using swirl-based parameters. Leibovich [28] explained a vortex breakdown as a change in the structure of the vortex initiated by a variation in the ratio between tangential velocity components and axial velocity components.

In a similar vein, Ito et al. [34], who undertook a theoretical study of unsteady and steady vortex breakdown, proposed an interpretive criterion based on the use of the Rossby number (or inverse swirl parameter) defined as

$$\mathrm{Ro} = V/(r\Omega) \tag{1}$$

in which V, r, and Ω represent characteristic velocity, length, and rotation rate scales.

The breakdown criterion based on the Rossby number was completed by Spall et al. [17], who proposed scale definitions for the velocity distribution consistent with swirling flows, leading-edge vortices, and unconfined trailing wing-tip vortices. These definitions were adopted in the present study in the context of a confined tip-leakage vortex, which is typical of axial decelerating turbomachinery. In detail, the following scales were used.

- r was taken to be the radial distance from the vortex axis at which the swirl velocity was at its maximum, in accord with the characteristic viscous length scale suggested by Leibovich [35].
- $V = w_{a\mathrm{TLV}}$ was taken to be the axial velocity at r.
- Ω was taken to be the rotation rate in the wing-tip vortices due to the solid body rotationlike structure (estimated near the vortex center).

The choice of $w_{a\mathrm{TLV}}$ as a velocity scale was consistent with the swirl scale $\Omega r = w_{p\mathrm{TLV}}$ and the critical Ro number values mentioned in the relevant literature. This ranged from 0.64 for a confined axisymmetric vortex breakdown [36] to 0.6 for wing-tip vortices with bubble or spiral type vortex breakdown [37].

The chordwise distributions of the tip-leakage vortex Rossby numbers for the data rotor and the AC90/6/TF rotor under design operating conditions, Fig. 5, indicate that the AC90/6/TF fan featured a vortex breakdown and confirm that the unseparated bubble core at midchord (as previously illustrated in Fig. 2) corresponded to the attainment of the Rossby number critical value. This finding provides evidence for the validity of the Rossby breakdown concept in assessing the swirling flows of axial rotor turbomachinery [38].

The findings with respect to chordwise Ro distributions also indicate that the trend in the Rossby number, as it approached the critical value, was related to an incipient breakdown. Ro values below the critical threshold are apparent, Fig. 5, for both the data rotor and the AC90/6/TF rotor. The Ro distributions also reveal that the approach to the breakdown is driven by a similar chordwise descent of the vortex rotation number. This suggests that the control of the tip-leakage vortex Rossby number could be based on a near-axis swirl supply or subtraction, which could be implemented by a modification of the end-plate configuration with a view to establishing an original design concept for blade-tip aerodynamic appendages.

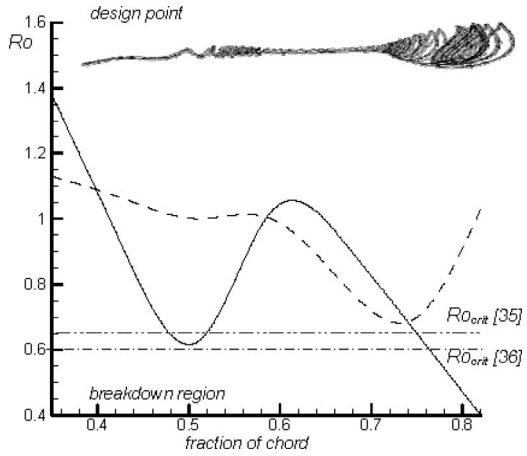

Fig. 5 Chordwise distributions of tip-leakage vortex rotation Ro number at design operating point (dashed line: data fan; solid line: AC90/6/TF fan)

Downloaded 28 May 2010 to 128.113.26.88. Redistribution subject to ASME license or copyright; see http://www.asme.org/terms/Terms_Use.cfm

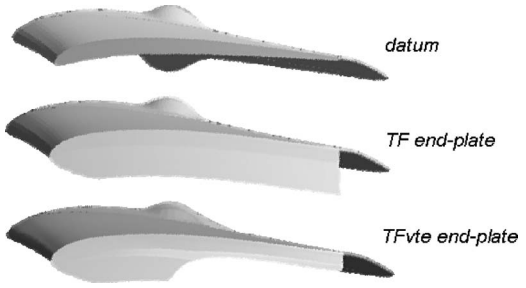

Fig. 6 AC90/6TF and AC90/6TFvte end-plate geometries (not to scale) [16]

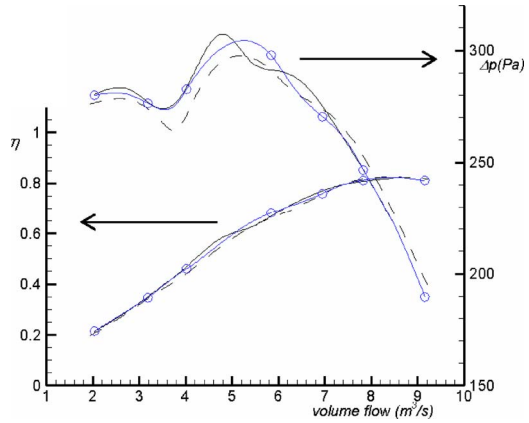

Fig. 7 Measured total pressure and total pressure efficiency characteristic curves (dashed lines: data fan; solid lines: AC90/6/TF fan; line-circles: AC90/6/TFvte fan)

4 Tip End-Plate Design Concept

To suppress the tip-leakage vortex-bursting phenomenon in the operation of the AC90/6/TF fan rotor, a new end-plate design was recently proposed [16,39] here labeled as AC90/6/TFvte. The proposed configuration controls the onset of vortex breakdown by means of an end-plate of variable chordwise thickness. The aim of the new concept is to enhance near-axis swirl [19,20] by reconfiguring the end-plate at the tip with a view to influencing the momentum transfer from the leakage flow and to force some waviness into the leakage vortex trajectory, as suggested by Srigrarom and Kurosaka [21] in the delta-wing platform design. According to the analysis of tip-leakage vortices in terms of the Rossby number behavior, Fig. 4, the shape of the end-plate is based on the definition of a safe rotation number chordwise gradient.

The rationale of the present investigation was to compute the end-plate thickness distribution ($t_{ep}(s_c)$) by combining a simplified law for the tip-gap pressure drop with a stability criterion of the TLV by prescribing a safe chordwise distribution of the vortex Rossby number, Fig. 5. The pressure losses within the tip gap at each chordwise abscissa s_c were modeled by studying the leakage flow as a two-dimensional flow orthogonal to the chord line. The pressure drop could thus be expressed as a function of the following:

- the geometry of the gap (height τ_{gap} and width t_{ep})
- the kinetic energy of the leakage flow, as given by the leakage velocity component normal to the chord $(w_{Ln})^2$
- the friction factor f_f, which is itself a function of the leakage flow Reynolds number $\mathrm{Re}_{gap}=f$ (τ_{gap} and w_{Ln} velocity scale) and
- the end-plate thickness $t_{ep}(s_c)$

Details concerning the design concept are given in Ref. [39].

5 Assessment of End-Plate Aerodynamics

Experimental quantitative studies were carried out to assess the aerodynamic performance of the modified end-plate configuration of AC90/6/TFvte compared with the data fan and the AC90/6/TF fan (Fig. 6). The studies were conducted in the ducted configuration under near-design conditions.

5.1 Aerodynamic Performance. The main performance parameters were the fan total pressure and the efficiency. Measurements of static and dynamic pressure were carried out with four taps, equally spaced on the casing wall, and a standard Pitot-probe. The probe was mounted on a traverse mechanism fixed to the outer wall of the test rig. A Furness digital multichannel micromanometer (Model FC012, Furness Controls Ltd., UK) with a 2 kPa range and a resolution of 1 Pa was used to read pressure data. The pressure measurement accuracy was ±0.5% of read data. The efficiency was calculated as the ratio between the air power (computed on either static or dynamic pressure rise) and the electric power. The absorbed electric power was measured with an ac power analyzer having an accuracy of 0.24% of read data.

The total pressure and efficiency curves for the data rotor, the AC90/6/TF rotor, and the AC90/6/TFvte, Fig. 7, revealed a small performance reduction in the AC90/6/TF rotor as a result of the interaction of the large vortex structure at the tip clearance with the suction side (SS) near the surface fluid [35]. However, this diminution in performance was not apparent in the AC90/6/TFvte rotor, in which the static pressure rise increased by throttling the rotor toward the peak pressure.

A comparison of the efficiency curves revealed that both of the modified rotors demonstrated an improvement in efficiency when the volume flow rate was greater than the design setting. The efficiency curves also indicate that the adoption of the tip end-plates resulted in the appearance of an efficiency plateau, which shifted the peak efficiency volume flow rate toward the rotor stall margin.

The rotor performance was quantitatively assessed along the operating line and compared with the experimental data in terms of static pressure rise and efficiency (η_{stat}) computed in terms of static pressure rise, Table 4.

The parameters for prediction of performance refer to axial sections located at (i) the inlet of the domain and (ii) 20% midspan chords downstream of the blade's trailing edge. The findings confirmed the predicted performance.

5.2 Leakage Flow Survey. The effects of the various end-plate configurations on leakage flow were assessed with a view to ascertaining how these features related to the control of leakage vortex swirl.

The chordwise distribution of the tip-leakage vortex Rossby number Ro for the AC90/6/TFvte rotor was compared with that for the AC90/6/TF rotor, Fig. 8. The Ro distribution for the new end-plate with variable thickness indicated that the leakage vortex

Table 4 Predicted and measured fans static overall performance

	Measurements		Predictions	
	Δp_{stat} (Pa)	η_{stat}	Δp_{stat} (Pa)	η_{stat}
Data	134.8	0.49	133.3	0.510
AC90/6/TF	126.2	0.51	126.1	0.504
AC90/6/TFvte	129.0	0.52	128.2	0.516

Downloaded 28 May 2010 to 128.113.26.88. Redistribution subject to ASME license or copyright; see http://www.asme.org/terms/Terms_Use.cfm

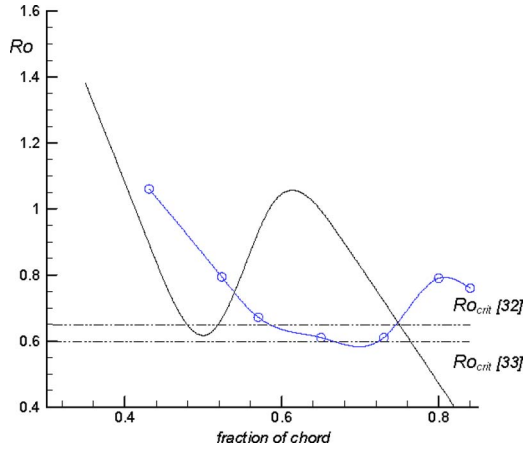

Fig. 8 Chordwise distributions of tip-leakage vortex rotation Ro number at design operating point (line: AC90/6/TF fan; line-circle: AC90/6/TFvte fan)

rotation number decreased at a reduced rate, reaching the critical Ro region at about 0.6 chords. It is also apparent that the end-plate thickness reduction from midchord exerted effective control on the swirl level of the leakage vortex that appears in the aft of the blade tip.

Control of tip-leakage vortex rotation on the basis of near-axis swirl supply was effectively obtained by adopting a nonconstant end-plate configuration, Fig. 8.

To provide additional information on these phenomena, Fig. 9 compares the leakage velocity (w_{LV}, defined as the velocity normal to the chord) and the leakage-flow skewing angle (β_{LV}) in the chordwise direction. The w_{LV} and β_{LV} profiles through the gap were plotted at various chordwise positions downstream from the leading edge: at 0.15 chords (Fig. 9(*a*)), at 0.3 chords (Fig. 9(*b*)), at 0.55 chords (Fig. 9(*c*)), and at 0.75 chords (Fig. 9(*d*)). It should be noted that the leakage velocity (w_{LV}) was normalized by using the bulk velocity.

Although the data rotor and the TF rotor had similar onset of leakage flow, it is apparent from the velocity distributions of the TFvte blade in proximity to the leading edge (Fig. 9(*c*)) that the leakage jet was not present at 0.15 chords in this variable-thickness configuration. This finding appears to be correlated with the leakage-flow skewing-angle distribution (underturned at the blade tip and overturned at the casing).

At about 0.3 chords (Fig. 9(*b*)), the TFvte velocity profile suggested that the leakage flow originated from the blade tip. Moreover, in the same position, the TF rotor appeared to control the leakage velocity distribution by reducing w_{LV} at the higher radii. It should also be noted that the velocity distributions indicated the presence of a clear separation at the tip, as indicated by the presence of a tip-separation vortex.

At the midchord (Fig. 9(*c*)), as a result of the reduction in tip appendage thickness in the TFvte configuration, the velocity profile provided evidence of an augmented momentum transfer to the leakage flow already rolled up into a vortex. This in-axis swirl supply was obtained with a slight increase in the skewing angle.

In the aft portion of the blade (Fig. 9(*d*)), the variable thickness end-plate was shown to increase the velocity close to the casing and, simultaneously, to reduce the skewing angle at which the flow leaked and supplied the vortex core.

Control of the leakage flow phenomena as a result of the adoption of the improved tip configurations was also assessed by comparing the predicted tip-leakage mass flows for the tested operating point, Table 5.

The predicted leakage flow rates confirmed that the new end-plate produced identical control of the leakage flow as compared with the TF configuration.

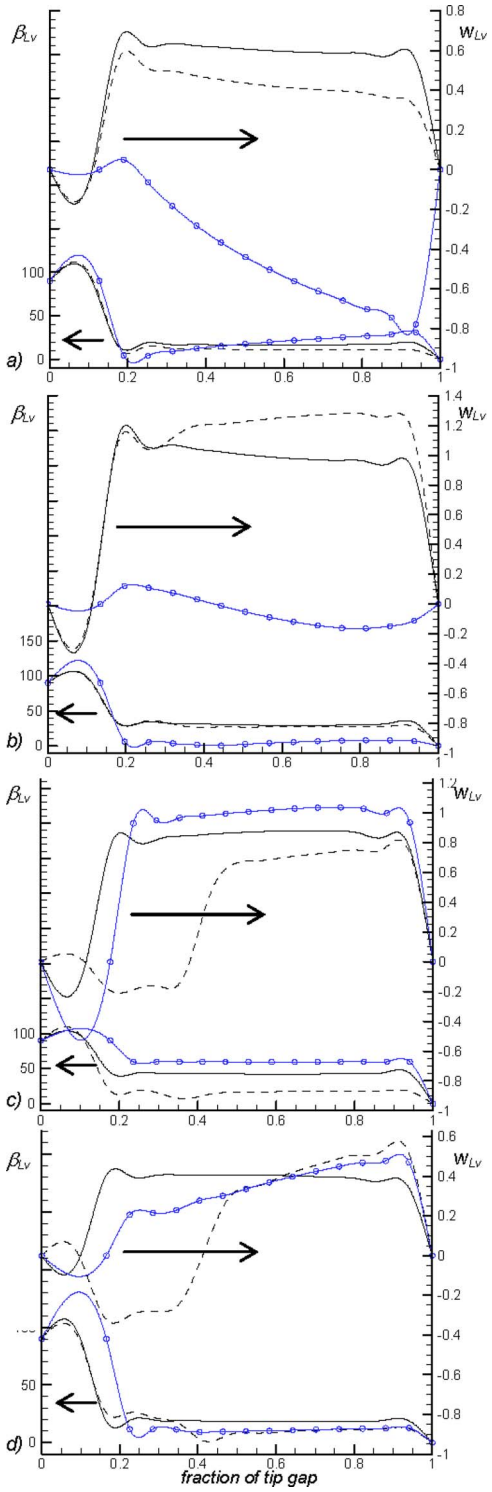

Fig. 9 Tip leakage flow velocity and skewing angle distributions through the gap: (*a*) 0.15 chord, (*b*) 0.3 chord, (*c*) 0.55 chord, and (*d*) 0.75 chord (dashed lines: data fan; solid lines: AC90/6/TF fan; line-circles: AC90/6/TFvte fan)

5.3 Influence of Spanwise Rotor Flow Behavior. The presence of the tip-appendages was found to influence the spanwise re-arrangement of flow in rotor blade passages.

Figure 10 compares the pitch-averaged distributions of axial (φ_a) and radial (φ_r) flow coefficients behind the rotor on an axial plane 1.2 chord downstream the blade leading edge. The main evidence of the role played by the end-plates along the span was

Downloaded 28 May 2010 to 128.113.26.88. Redistribution subject to ASME license or copyright; see http://www.asme.org/terms/Terms_Use.cfm

Table 5 Predicted tip-leakage mass flow

	Data rotor	AC/90/6/TF rotor	AC/90/6/TFvte rotor
	Leakage flow/inflow (%)	Leakage flow/inflow (%)	Leakage flow/inflow (%)
D point	1.40	1.03	0.95

given by the axial flow coefficient profiles. The adoption of TF or TFvte geometrics to control the leakage flow resulted in healthier boundary layers at the blade root. The reduced fluid centrifugation on blade pressure surface, consequence of the end-plate, contributed to the suppression of the hub separation bubble featuring data rotor aerodynamic behavior.

On the other hand, the radial re-arrangement throughout the vane was also partially affected by the blade configuration at the tip.

In Fig. 10, the radial flow coefficient profiles for TF and TFvte blades featured a reduction in the inward peak velocity at the higher radii compared with the data distribution. Moreover, the TFvte behavior in the proximity of the tip, featuring higher outward radial velocities, appeared in accordance with the design criteria of this end-plate based on the control of leakage vortex swirl.

When looking at the work distribution along the span as measured by the swirl coefficient ψ, Fig. 11, it was shown that the tip appendages aerodynamics was not driven by blade unloading. As far as the TF distribution was concerned, it featured a localized swirl reduction on the outer end-wall as a consequence of the discussed tip vortex bursting, whereas the TFvte swirl profile showed that the end-plate geometry modification succeeded in recovering the aerodynamic performance penalty given by the presence of the aerodynamic appendages already demonstrated by the test, Fig. 7.

Rotor loss behavior at the blade tip was investigated under near-design conditions (*D* point) in terms of the local total loss coefficient (ζ), which was defined as

$$\zeta = \bar{p}_{0\text{in}} - p_0/0.5\rho\bar{w}_{\text{in}}^2 \tag{2}$$

in which p_0 is the local total pressure and $\bar{p}_{0\text{in}}$ and $0.5\rho\bar{w}_{\text{in}}^2$ are, respectively, the reference pitch-averaged relative total and dynamic pressures computed at the inlet midspan plane.

The total loss coefficient distribution within the blade passage was obtained by probing the flow fields in the vicinity of the blade's leading edge at about midchord and in the region behind the blade (at approximately 25%, 65%, and 120% chords from the leading edge).

The predicted loss evolutions under design operating conditions, as shown in Figs. 12(*a*)–12(*c*), were in accordance with previous studies of low-speed rotors [23] and with the other aerodynamic tests carried out in the present study. At the rotor inlet, all rotor distributions demonstrated loss cores that were mainly concentrated on the hub annulus walls. Moving toward the aft of the

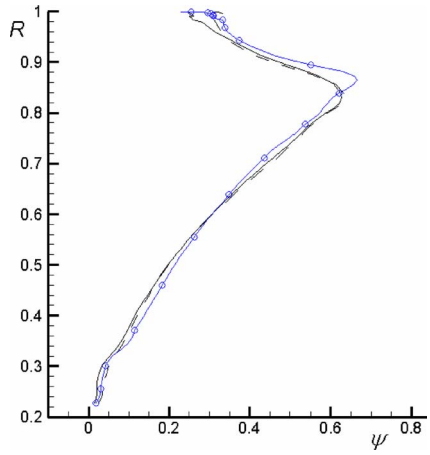

Fig. 11 Spanwise distributions of swirl flow coefficient behind the rotor (dashed lines: data fan; solid lines: AC90/6/TF fan; line-circles: AC90/6/TFvte fan)

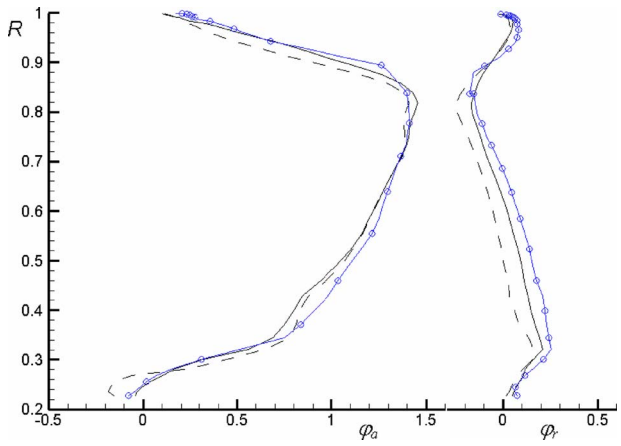

Fig. 10 Spanwise distributions of axial (φ_a) and radial (φ_r) flow coefficients behind the rotor (dashed lines: data fan; solid lines: AC90/6/TF fan; line-circles: AC90/6/TFvte fan)

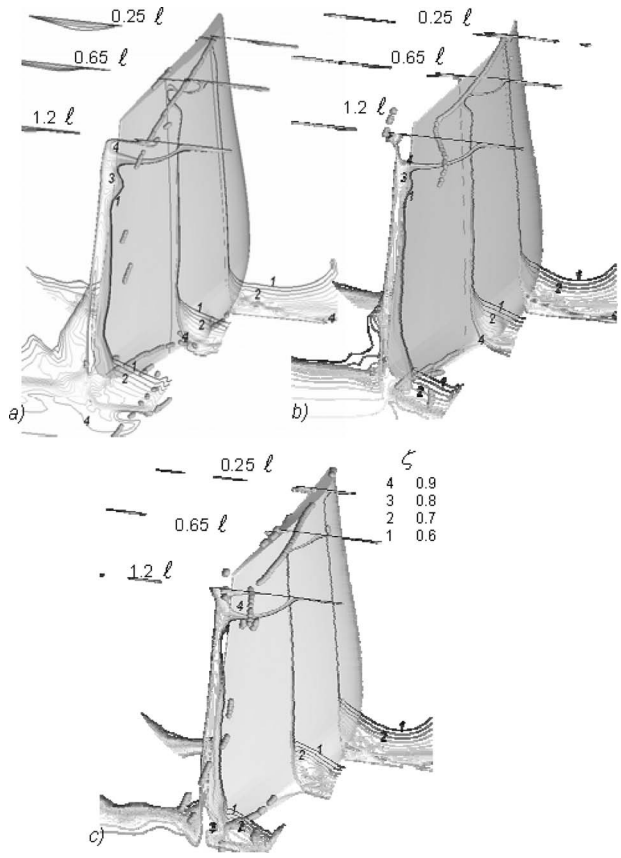

Fig. 12 Evolution of total pressure loss coefficient ζ inside the blade passage: (*a*) data rotor, (*b*) AC90/6/TF rotor, and (*c*) AC90/6/TFvte

Downloaded 28 May 2010 to 128.113.26.88. Redistribution subject to ASME license or copyright; see http://www.asme.org/terms/Terms_Use.cfm

blade, the loss maps were characterized by loss core directly related to the development of primary tip vortices traveling through the blade vane. As a result of the vortex breakdown, a larger peak loss core was associated with the modified tip configuration of the AC90/6/TF rotor (Fig. 12(*b*)). A comparison of the AC90/6/TF rotor and the data rotor loss map at 1.2ℓ revealed that the improved tip rotor featured a beneficial spanwise loss distribution; it outperformed the data fan within the wake and on the hub endwall where it provided healthier near-wall layers on pressure and suction side corners.

With regard to the AC90/6/TFvte fan rotor (Fig. 12(*c*)), there was evidence that the leakage vortex breakdown was able to reduce the high loss core at the tip—both behind the rotor and along the blade suction side within the interaction region between leakage and near surface flows. This can be considered to be a consequence of the reduced 3D flow re-arrangement occurring as a result of the reduction in mass leaking through the tip gap. The limited radial migration of near-wall surface fluid induced smaller hub loss core and the contraction of suction/corner stall (Figs. 12(*b*) and 12(*c*)).

6 Conclusions

The aim of the present study was to test a modified tip configuration that was developed to control leakage-flow phenomena and rotor aero-acoustic signatures in a family of axial flow fans. The passive control technique explored in the study was based on blade tips that were modified by the addition of antivortex appendages as end-plates. The end-plate configuration aimed to control the chordwise evolution of the leakage vortex swirl level by preventing the occurrence of tip-leakage vortex bursting by the enhancement of near-axis swirl. Two configurations were investigated: (i) an end-plate with constant thickness and (ii) an end-plate with a variable thickness distribution according to the concept of a safe rotation number chordwise gradient.

The aerodynamic tests reported here indicate that the original tip concept demonstrated reduced performance along the operating line. The leakage-flow survey has shown that the variable-thickness configuration was able to exert control over near-axis leakage vortex swirl. As a result, although the critical Rossby number region is reached, the end-plate configuration provides effective control over leakage vortex bursting.

The analysis of the spanwise flow behavior shows that the presence of the end-plates resulted in a beneficial aerodynamic behavior along the blade span, in particular, featuring the control on the hub corner separation.

The loss coefficient distributions confirm that the highest loss regions were always observed in coincidence with the leakage vortex core with a nearly constant peak loss value. The comparative loss behavior was in accordance with the aerodynamic test results, and the overall efficiency gain for the investigated end-plates was found to be a consequence of the reduced 3D flow re-arrangement caused by the improved tip configurations.

Acknowledgment

The present research was undertaken in the context of a contract (Contract No. FW-DMA06-09) between Fläkt Woods Ltd. and the Dipartimento di Meccanica e Aeronautica, Sapienza University of Rome. A.C. and F.R. acknowledge the assistance provided by the Italian Ministry for Academic Research (MIUR), which was provided under the auspices of the Ateneo and Facoltà 2006 projects. The contribution of Iain Kinghorn to the experiments is also gratefully acknowledged.

Nomenclature

BPF = blade passing frequency
C_p = static pressure coefficient $((p-\bar{p}_{\text{in}})/0.5\rho U_c^2)$
dE_m = nondimensional mechanical energy loss through the gap
H_n = normalized helicity $(\xi_i w_i/|\xi||w|)$
k = turbulent kinetic energy
ℓ = blade chord
PS = pressure side
p = static pressure
r = radius
R = nondimensional radius (r/r_c)
t = blade pitch
U_c = casing relative peripheral velocity
V = volume flow rate
v, w = absolute and relative velocities, respectively
x, y, and z = Cartesian coordinates

Greek Symbols

ε = turbulent dissipation rate
ζ = total loss coefficient $(\bar{p}_{0\text{in}}-p_0/0.5\rho\bar{w}_{\text{in}}^2)$
η = efficiency
ν = hub-to-casing diameter ratio
ξ_i = vorticity vector
σ = blade solidity
Φ = global flow coefficient (annulus area-averaged axial velocity normalized by U_c)
φ_a = axial flow coefficient
φ_r = radial flow coefficient
ψ = swirl flow coefficient
χ = rotor tip clearance (% of the span)
ω = rotor angular velocity

References

[1] Fukano, T., and Takamatsu, Y., 1986, "The Effects of Tip Clearance on the Noise of Low-Pressure Axial and Mixed Flow Fans," J. Sound Vib., **105**, pp. 291–308.
[2] Furukawa, M., Inoue, M., Kuroumaru, M., Saiki, K., and Yamada, K., 1999, "The Role of Tip Leakage Vortex Breakdown in Compressor Rotor Aerodynamics," ASME J. Turbomach., **121**, pp. 469–480.
[3] Storer, J. A., and Cumpsty, N. A., 1991, "Tip Leakage Flow in Axial Compressors," ASME J. Turbomach., **113**, pp. 252–259.
[4] Ganz, U. W., Joppa, P. D., and Scharpf, D. F., 1998, Boeing 18-Inch Fan Rig Broadband Noise Test, NASA Report No. CR-1998-208704.
[5] Takata, H., and Tsukuda, Y., 1977, "Stall Margin Improvement by Casing Treatment—Its Mechanism and Effectiveness," ASME J. Eng. Power, **99**, pp. 121–133.
[6] Smith, G. D. J., and Cumpsty, N. A., 1984, "Flow Phenomena in Compressor Casing Treatment," ASME J. Eng. Gas Turbines Power, **106**, pp. 532–541.
[7] Thompson, D. W., King, P. I., and Rabe, D. C., 1998, "Experimental and Computational Investigation on Stepped Tip Gap Effects on the Flowfield of a Transonic Axial-Flow Compressor Rotor," ASME J. Turbomach., **120**, pp. 477–486.
[8] Jensen, C. E., 1986, "Axial-Flow Fan," U.S. Patent No. 4,630,993.
[9] Quinlan, D. A., and Bent, P. H., 1998, "High Frequency Noise Generation in Small Axial Flow Fans," J. Sound Vib., **218**, pp. 177–204.
[10] Longet, C. M. L., 2003, "Axial Flow Fan With Noise Reducing Means," U.S. Patent No. 2003/0123987 A1.
[11] Mimura, M., 2003, "Axial Flow Fan," U.S. Patent No. 6,648,598 B2.
[12] Uselton, R. B., Cook, L. J., and Wright, T., 2005, "Fan With Reduced Noise Generation," U.S. Patent No. 2005/0147496 A1.
[13] Corsini, A., Perugini, B., Rispoli, F., Kinghorn, I., and Sheard, A. G., 2006, "Investigation on Improved Blade Tip Concept," ASME Paper No. GT2006-90592.
[14] Corsini, A., Rispoli, F., and Sheard, A. G., 2007, "Development of Improved Blade Tip Endplate Concepts for Low-Noise Operation in Industrial Fans," Proc. Inst. Mech. Eng., Part A, **221**(5), pp. 669–681.
[15] Corsini, A., Perugini, B., Rispoli, F., Kinghorn, I., and Sheard, A. G., 2007, "Experimental and Numerical Investigations on Passive Devices for Tip-Clearance Induced Noise Reduction in Axial Flow Fans," *Proceedings of the Seventh European Conference on Turbomachinery*, Athens, Greece.
[16] Corsini, A., Rispoli, F., and Sheard, A. G., 2008, "A Meridional Fan," Patent Application No. GB 0800582.9, pending.
[17] Spall, R. E., Gatski, T. B., and Grosch, C. E., 1987, "A Criterion for Vortex Breakdown," Phys. Fluids, **30**(11), pp. 3434–3440.
[18] Escudier, M., 1987, "Confined Vortices in Flow Machinery," Annu. Rev. Fluid Mech., **19**, pp. 27–52.
[19] Herrada, M. A., and Shtern, V., 2003, "Vortex Breakdown Control by Adding Near-Axis Swirl and Temperature Gradients," Phys. Rev. E, **68**, p. 041202.
[20] Jones, M. C., Hourigan, K., and Thompson, M. C., 2001, "The Generation and Suppression of Vortex Breakdown by Upstream Swirl Perturbations," *Proceedings of the 14th Australian Fluid Mechanics Conference*, Adelaide, Australia.
[21] Srigrarom, S., and Kurosaka, M., 2000, "Shaping of Delta-Wing Planform to

Downloaded 28 May 2010 to 128.113.26.88. Redistribution subject to ASME license or copyright; see http://www.asme.org/terms/Terms_Use.cfm

Suppress Vortex Breakdown," AIAA J., **38**, pp. 183–186.
[22] Inoue, M., Kuroumaru, M., and Furukawa, M., 1986, "Behavior of Tip Leakage Flow Behind an Axial Compressor Rotor," ASME J. Eng. Gas Turbines Power, **108**, pp. 7–14.
[23] Corsini, A., and Rispoli, F., 2004, "Using Sweep to Extend Stall-Free Operational Range in Sub-Sonic Axial Fan Rotors," Proc. Inst. Mech. Eng., Part A, **218**, pp. 129–139.
[24] Borello, D., Corsini, A., and Rispoli, F., 2003, "A Finite Element Overlapping Scheme for Turbomachinery Flows on Parallel Platforms," Comput. Fluids, **32**(7), pp. 1017–1047.
[25] Craft, T. J., Launder, B. E., and Suga, K., 1996, "Development and Application of a Cubic Eddy-Viscosity Model of Turbulence," Int. J. Heat Fluid Flow, **17**, pp. 108–155.
[26] Corsini, A., Rispoli, F., and Santoriello, A., 2005, "A Variational Multi-Scale High-Order Finite Element Formulation for Turbomachinery Flow Computations," Comput. Methods Appl. Mech. Eng., **194**(45–47), pp. 4797–4823.
[27] Lucca-Negro, O., and O'Doherty, T., 2001, "Vortex Breakdown: A Review," Prog. Energy Combust. Sci., **27**, pp. 431–481.
[28] Leibovich, S., 1978, "The Structure of Vortex Breakdown," Annu. Rev. Fluid Mech., **10**, pp. 221–246.
[29] Escudier, M., and Zehnder, N., 1982, "Vortex Flow Regimes," J. Fluid Mech., **115**, pp. 105–121.
[30] Inoue, M., and Furukawa, M., 2002, "Physics of Tip Clearance Flow in Turbomachinery," ASME Paper No. FEDSM2002-31184.
[31] Leibovich, S., 1982, "Wave Propagation, Instability, and Breakdown of Vortices," *Vortex Motion*, M. Hornung, ed., Braunschweig, Vieweg, pp. 50–67.
[32] Benjamin, T. B., 1962, "Theory of the Vortex Breakdown Phenomenon," J. Fluid Mech., **14**, pp. 593–629.
[33] Tsai, C.-Y., and Widnall, S. E., 1980, "Examination of Group-Velocity Criterion for Breakdown of Vortex Flow in a Divergent Duct," Phys. Fluids, **23**, pp. 864–870.
[34] Ito, T., Suematsu, Y., and Hayase, T., 1985, "On the Vortex Breakdown Phenomena in a Swirling Pipe-Flow," Nagoya University, Faculty of Engineering, Memoirs, **37**(2), pp. 117–172.
[35] Leibovich, S., 1984, "Vortex Stability and Breakdown: Survey and Extension," AIAA J., **22**, pp. 1192–1206.
[36] Uchida, S., Nakamura, Y., and Ohsawa, M., 1985, "Experiments on the Axisymmetric Vortex Breakdown in a Swirling Air Flow," Trans. Jpn. Soc. Aeronaut. Space Sci., **27**(78), pp. 206–216.
[37] Garg, A. K., and Leibovich, S., 1979, "Spectral Characteristics of Vortex Breakdown Flowfields," Phys. Fluids, **22**(11), pp. 2053–2064.
[38] Gbadebo, S. A., Cumpsty, N. A., and Hynes, T. P., 2006, "Interaction of Tip Clearance Flow and Three-Dimensional Separations in Axial Compressors," ASME Paper No. GT2006-90071.
[39] Corsini, A., and Sheard, A. G., 2007, "Tip End-Plate Concept Based on Leakage Vortex Rotation Number Control," Comput. Appl. Math., **8**(1), pp. 21–37.

Downloaded 28 May 2010 to 128.113.26.88. Redistribution subject to ASME license or copyright; see http://www.asme.org/terms/Terms_Use.cfm